

Nondipole Coulomb sub-barrier ionization dynamics and photon momentum sharing

Pei-Lun He,^{*} Michael Klaiber, Karen Z. Hatsagortsyan,[†] and Christoph H. Keitel
Max-Planck-Institut für Kernphysik, Saupfercheckweg 1, 69117 Heidelberg, Germany

(Dated: October 12, 2021)

The nondipole under-the-barrier dynamics of the electron during strong-field tunneling ionization is investigated, examining the role of the Coulomb field of the atomic core. The common analysis in the strong field approximation is consequently generalised to include the leading light-front non-dipole Coulomb corrections and demonstrates the counter-intuitive impact of the sub-barrier Coulomb field. Despite its attractive nature, the sub-barrier Coulomb field increases the photoelectron nondipole momentum shift along the laser propagation direction, involving a strong dependence on the laser field. The scaling of the effect with respect to the principal quantum number and angular momentum of the bound state is found. We demonstrate that the signature of Coulomb induced sub-barrier effects can be identified in the asymptotic photoelectron momentum distribution via a comparative study of the field-dependent longitudinal momentum shift for different atomic species with state-of-the-art experimental techniques of mid-infrared lasers.

Exchanges of photon's energy, momentum, and angular momentum with charged particles are fundamental building blocks of light-matter interactions. In the presence of an intense laser field, photon energy absorption can trigger nonlinear processes like high-order harmonic generation [1, 2], above-threshold ionization [3], and nonsequential double ionization [4]. Meanwhile, the angular momentum transfer from the laser beam is vital for generating vortex light [5, 6], polarized electrons [7, 8] and positrons [9], and nuclei vortices [10]. The absorption of the photon momentum has attracted considerable interest recently due to various breakthroughs in experimental technique [11–18]. High precision measurements raised questions on how the absorbed photon momentum is partitioned between the photoelectron and the parent ion. The analysis relies on investigating the photoelectron momentum distribution (PMD) along the laser propagation direction. The coincidence measurement of the photoelectron and its parent ion provides a direct check of the momentum conservation law in the microscopic world [19].

It follows from energy-momentum conservation that in the simple-man model of tunneling ionization [2], when the electron appears in the continuum with a vanishing momentum due to a circularly polarized laser pulse, the total absorbed photon momentum is shared between the ion and electron as I_p/c and U_p/c , respectively [11, 20], where I_p is the ionization energy, U_p the ponderomotive potential, and c the speed of light. However, in deviation to the simple-man picture, there is a longitudinal momentum transfer to the electron during tunneling due to the laser Lorentz force $\delta p_z \sim (\kappa/c)B_0\tau \sim I_p/c$, where $\kappa = \sqrt{2I_p}$ is the atomic velocity, $\tau = \gamma/\omega$ the tunneling formation time, $\gamma = \omega\kappa/E_0$ the Keldysh parameter, E_0 , B_0 , and ω are the laser electric, and magnetic fields, and its frequency, respectively. Atomic units are used throughout. Then, the most probable electron longitudinal momentum at the tunnel exit becomes $I_p/(3c)$ [21],[14]. This is the case for a short-range atomic potential, when the electron begins the sub-barrier motion at the bound

state with a longitudinal momentum $v_{zs} = -2I_p/(3c)$ [21, 22]. The Coulomb field of the atomic core reshapes the tunneling barrier and, consequently, the nondipole momentum shift due to the sub-barrier dynamics. The latter is also affected by the momentum distribution of the bound state, which contributes into the birth probability of the quantum orbit.

The long-range character of the Coulomb field of the atomic core is known to play a key role in strong-field ionization. It enhances the tunneling probabilities [23–25]. In the continuum, it is responsible for the low-energy [26–32] and high-energy structures [33, 34] in the PMD and the interplay between nondipole and Coulomb effects [12, 13, 35–38]. The sub-barrier dynamics can induce specific effects in tunneling ionization [7, 8, 21, 39, 40]. For instance, the sub-barrier nonadiabatic dynamics results in a transverse momentum shift and polarized photoelectrons [7, 8]. The sub-barrier Coulomb effect can induce a phase shift of the quantum orbit [39], disturbing the holography pattern. However, there is yet no conclusion on how the under-the-barrier Coulomb action affects the nondipole momentum shift. While simulations via the time-dependent Schrödinger equation (TDSE) [41–43] and time-dependent Dirac equation [16] give accurately the final longitudinal momentum shift, they do not provide intuitive insight on the underlying sub-barrier dynamics.

In this Letter, we investigate the electron's sub-barrier nondipole dynamics in strong-field tunneling ionization within an enhanced analytical description including the role of the Coulomb field of the atomic core. The sub-barrier dynamics is described within the light-front [44] nondipole Coulomb-corrected strong-field approximation (SFA), while the continuum one via the light-front nondipole classical trajectory Monte Carlo (CTMC) simulation, disentangling the effect of the sub-barrier Coulomb action from that in the continuum. We found that the sub-barrier Coulomb effect induces an increase of the photoelectron nondipole longitudinal momentum shift, and discuss its counterintuitive physical origin. The depen-

dence of the Coulomb effect on the angular momentum of the bound state is analyzed. Finally, we discuss how the Coulomb effects in the sub-barrier nondipole momentum shift can be observed experimentally using mid-infrared laser fields.

Our description of the tunneling process is based on TDSE in the Göppert-Mayer gauge [45]

$$i \frac{\partial}{\partial t} \psi(\mathbf{x}, t) = \left[\frac{1}{2} (\mathbf{p} + \mathbf{A}(\mathbf{x}, \eta))^2 + V(\mathbf{x}) - \phi(\mathbf{x}, \eta) \right] \psi(\mathbf{x}, t), \quad (1)$$

where $V(\mathbf{x}) = -\frac{Z}{|\mathbf{x}|}$ is the Coulomb potential of the atomic core, $A^\mu = (\phi, \mathbf{A})$ the laser four-vector potential in the Göppert-Mayer gauge, with $\phi = -\mathbf{x} \cdot \mathbf{E}(\eta)$ and $\mathbf{A}(\mathbf{x}, \eta) = \hat{\mathbf{z}}\phi/c$, $\mathbf{E}(\eta) = E_0 [\hat{\mathbf{x}} \cos(\omega\eta) - \hat{\mathbf{y}} \sin(\omega\eta)] \exp\left(-2 \ln 2 \frac{\eta^2}{L^2}\right)$ the laser field of circular polarization with $L = 4 T$ and T is the optical cycle, and with the light-front coordinate $\eta = t - z/c$. The Hamiltonian in Eq. (1) is accurate up to the $1/c$ order, suitable in the considered parameter regime. The deviation from the fully relativistic theory [46–49] is given by I_p/c^2 terms for the sub-barrier and U_p/c^2 terms for the continuum dynamics. We apply light-front nondipole Coulomb-corrected SFA [50], which corresponds to the nondipole expansion of the relativistic theory [49]. The nondipole transition amplitude in the Göppert-Mayer gauge reads [51]:

$$M_{\mathbf{p}} = -i \int d\eta \frac{d^3\mathbf{x}}{(2\pi)^{3/2}} e^{-i \int_{\eta}^{\infty} d\eta' \frac{\frac{1}{2}\tilde{\mathbf{p}}(\eta')^2 + I_p}{1 - \frac{\tilde{p}_z}{c}}} \mathcal{F}_C^*(\eta, \mathbf{x}) \quad (2)$$

$$\times (1 - \tilde{p}_z/c) e^{-i\tilde{\mathbf{p}}(\eta) \cdot \mathbf{x}} \mathbf{E}(\eta) \psi_{\kappa lm}(\mathbf{x}),$$

where $\tilde{\mathbf{p}}(\eta) = (\mathbf{p}_\perp + \mathbf{A}_\perp(\eta), p_- - \frac{I_p}{c})$, with $p_- = p_z - \frac{\mathbf{p}_\perp^2}{2c}$ is the light-front momentum, $\mathbf{A}_\perp(\eta) \equiv -\int_{\infty}^{\eta} d\eta' \mathbf{E}(\eta')$, and $\psi_{\kappa lm}(\mathbf{x})$ is the bound state wave function. Note that $p_z/c \approx p_-/c \approx \tilde{p}_z/c$ up to the $1/c$ order. The use of the Göppert-Mayer gauge in the employed SFA is justified as it provides the accurate Coulomb corrected Perelomov-Popov-Terent'ev (PPT) ionization rate [23–25], which is well confirmed experimentally. The influence of the Coulomb field on the sub-barrier continuum electron is described by the Coulomb correction (CC) factor:

$$\mathcal{F}_C(\eta, \mathbf{x}) = \exp \left\{ i \int_{\eta}^{\infty} d\eta' V(\mathbf{x}(\eta, \eta')) / \left(1 - \frac{p_-}{c}\right) \right\}. \quad (3)$$

With saddle-point integration of Eq. (2), the differential ionization rate in the adiabatic regime is obtained [50]:

$$\Gamma^{(\nu, l, m)}(\eta, v_\perp, p_-) = \frac{\kappa}{\tilde{\kappa}} \frac{2^{2\nu+2} C_{\kappa l}^2 \kappa^{6\nu}}{(1 - \frac{p_-}{c})^{2\nu} E(\eta)^{2\nu}} \quad (4)$$

$$\times |Y_{lm}(\tilde{\mathbf{p}}(\eta_s))|^2 \exp \left[-\frac{2}{3} \frac{\tilde{\kappa}^3}{E(\eta)(1 - \frac{p_-}{c})} \right].$$

where (ν, l, m) are the atomic quantum numbers (the angular momentum projection is determined with respect

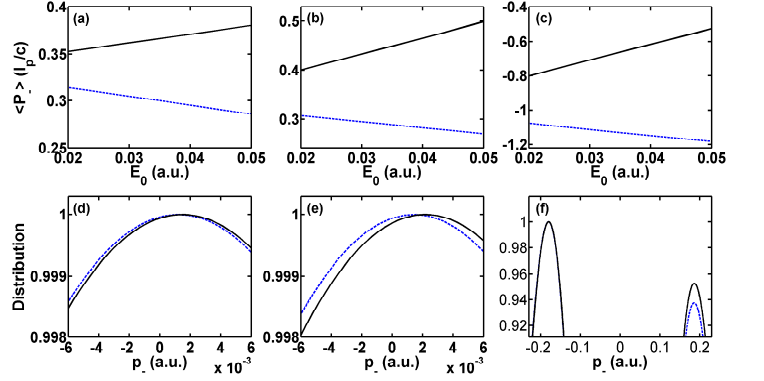


Figure 1. The sub-barrier Coulomb effect, neglecting the continuum influence, in the quasistatic regime: (a-c) The expectation value $\langle p_- \rangle$ vs E_0 ; (d-f) PMDs at the laser intensity $I = 10^{14}$ W/cm². The initial states are (a,d) hydrogen atom with quantum numbers (1, 0, 0), and argon atom (b,e) with (3, 1, 1), and (c,f) with (3, 1, 0). The solid-black line includes the sub-barrier Coulomb effect, while the dashed-blue line is the case of a short-range potential.

to the laser propagation axis), $E(\eta) = |\mathbf{E}(\eta)|$, $\tilde{\mathbf{p}}(\eta_s)$ is the saddle-point momentum, v_\perp the initial velocity component in the polarization plane, $C_{\kappa l}^2 = \frac{2^{2\nu-2}}{\nu(\nu+l)!(\nu-l-1)!}$, and $\tilde{\kappa} = \sqrt{\kappa^2 + \tilde{p}_z^2 + v_\perp^2}$. Nonadiabatic corrections do not change qualitatively our conclusion, see [50] (those without sub-barrier CC were considered in [52]).

To implement the light-front CTMC simulations, we sample over all possible ionization instants, tunneling exits, and initial momenta as initial conditions for the classic equation of motion

$$\frac{dQ}{d\eta} = \{Q, H\}, \quad \frac{dP}{d\eta} = \{P, H\}, \quad (5)$$

where $\{A, B\}$ is the Poisson bracket, with the canonical coordinates $Q = (x, y, z)$ and $P = (p_x, p_y, p_-)$. Trajectories are weighted by $\Gamma^{(\nu, l, m)}$ of Eq. (4). Accurate to the $1/c$ order, we have the classical light-front Hamiltonian

$$H = \frac{(\mathbf{p}_\perp + \mathbf{A}_\perp)^2 + (p_- + V/c)^2}{2 \left(1 - \frac{p_- + V/c}{c}\right)} + V. \quad (6)$$

The tunneling exit $\mathbf{x}^e = -\frac{I_p}{1 - p_-/c} \frac{\mathbf{E}(\eta)}{E(\eta)^2}$ is obtained by taking the real part of the complex trajectory [50].

Let us first discuss the sub-barrier Coulomb effect. Neglecting the Coulomb field effect in the continuum leads to the conservation of $P = (p_x, p_y, p_-)$. We plot the expectation value of p_- in Fig. 1. From Eq. (4), we derive $\langle p_- \rangle$ for an s -state in the leading order correction of E_0/E_a [50]:

$$\langle p_- \rangle = \frac{I_p}{c} \left[\frac{1}{3} + (2\nu - 1) \frac{E_0}{E_a} \right], \quad (7)$$

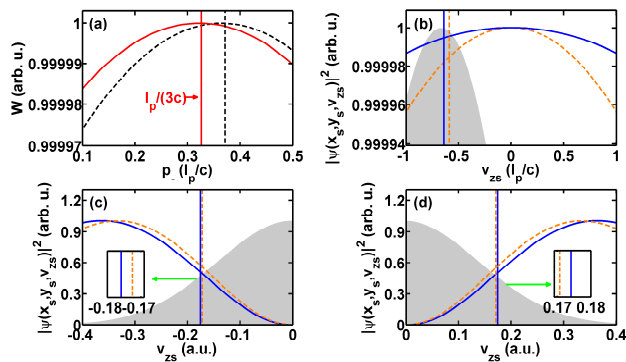


Figure 2. (a) The nondipole CC ionization window $\mathcal{W}(p_-) \equiv |\mathcal{F}_C|^2 \exp\left[-\frac{2}{3} \frac{\tilde{\kappa}^3}{E(\eta)(1-p_-/c)}\right]$: (solid-red) including the full sub-barrier dynamics, the peak is at $p_-^m \approx I_p/3c$ (solid-red gridline), (dashed-black) neglecting the sub-barrier z -dynamics, $p_-^m > I_p/3c$ (dashed-black gridline). The bound state wave functions at the starting point of the tunneling trajectory x_s : (b) for $(1, 0, 0)$ state, (c) for $(3, 1, 0)$ $v_{zs} < 0$, (d) for $(3, 1, 0)$ $v_{zs} > 0$; the wave function for the zero-range potential (solid-blue), and for the Coulomb case (dashed-orange); the tunneling window \mathcal{W} is shadowed; $E_0 = 0.04$ a.u. The gridlines in (b-d) indicate the peaks of $\mathcal{W}(v_{zs})|\psi(x_s, y_s, v_{zs})|^2$ with (dashed-orange), and without the sub-barrier CC (solid-blue).

with the atomic field $E_a = \kappa^3$. Note that the leading $I_p/(3c)$ term can be derived only employing the binding energy I_p and classical Lorentz sub-barrier dynamics in imaginary-time without any extra information about the binding potential and any time or spatial dependencies of the laser field, see Sec.IB.2 in [50]. Apart from the constant $I_p/(3c)$ [14, 21, 41, 51], the sub-barrier Coulomb effect yields an increase in the momentum shift, despite the attractive nature of the parent ion, and induces a strong dependence on the laser field and the principal quantum number of the bound state [Fig. 1].

The active electrons of most rare gas atoms are in the p -state. For instance, the ionization of the argon atom is dominated by signals from $(3, 1, \pm 1)$ orbits, while the nondipole shift for $(3, 1, 0)$ is more distinctive:

$$\langle p_- \rangle = \frac{I_p}{c} \left[-1 + (6\nu - 5) \frac{E_0}{E_a} \right]. \quad (8)$$

The physical origin of the Coulomb field effects for the nondipole sub-barrier dynamics is encoded in the exponent and the prefactor of the ionization amplitude of Eq. (2). The action contributed by the kinetic part, i.e. $\frac{1}{2} \frac{\tilde{\mathbf{p}}(\eta')^2 + I_p}{1 - \tilde{v}_z/c}$ of Eq. (2), gives the tunneling exponent in Eq. (4). Due to the laser magnetic field, the tunneling electron obtains a momentum in the laser propagation z -direction, which decreases the longitudinal tunneling energy and the tunneling probability, the latter being maximal at $p_-^m = I_p/(3c)$ [21]. We can estimate the contribution of the Coulomb action by evaluating Eq. (3)

with quantum orbits starting at the saddle point of the SFA-matrix element \mathbf{x}_s [53]. The momentum shift due to the sub-barrier Coulomb action \mathcal{F}_C is evaluated by the η -integration from the saddle-time η_s to the exit time $\eta_r = \text{Re } \eta_s$. When we include the full sub-barrier dynamics, motions along the tunneling channel (x -direction) as well as along the laser propagation direction (z -direction), then the CC factor \mathcal{F}_C does not change much the most probable momentum for the case of a short-range atomic potential $p_-^m = I_p/(3c)$ [54], see Fig. 2(a). Thus, the definition of the tunnel exit and the separation of η -integral in \mathcal{F}_C into the sub-barrier and continuum parts is not relevant for emerging of the sub-barrier CC. The essential sub-barrier CC for the nondipole momentum shift stems from matching the bound state wave function in the Coulomb field to the tunneling wave packet. The prefactor accounts for the probability of the quantum orbit, which originates at the bound state with the momentum v_{zs} . The width of the momentum space wave function $\psi_{klm}(x_s, y_s, v_{zs})$ (in the mixed representation, at the starting point of the ionization x_s) in the Coulomb field is narrower than that in the short-range potential, see Fig. 2(b). The most probable v_{zs}^m is the peak of the function: $|\psi(x_s, y_s, v_{zs})|^2 \mathcal{W}(v_{zs})$, which is indicated by the gridlines in Fig. 2 (b-d). The solid-red grid line in (b) includes the sub-barrier CC and is closer to the origin (larger v_{zs}), which yields an increase of the longitudinal momentum at the tunnel exit, as the total longitudinal momentum transfer from \mathbf{x}_s to \mathbf{x}^e is I_p/c .

The momentum shift and the corresponding CC depend essentially on the angular momentum of the bound state. We compare in Fig. 1 the expectation value of $\langle p_- \rangle$ with and without CC for quantum numbers $(1, 0, 0)$ (hydrogen) and $(3, 1, 0)$, $(3, 1, 1)$ (argon). There is a significant difference between s - and p -states. While the PMD of $(1, 0, 0)$ and $(3, 1, \pm 1)$ has only one peak, it has

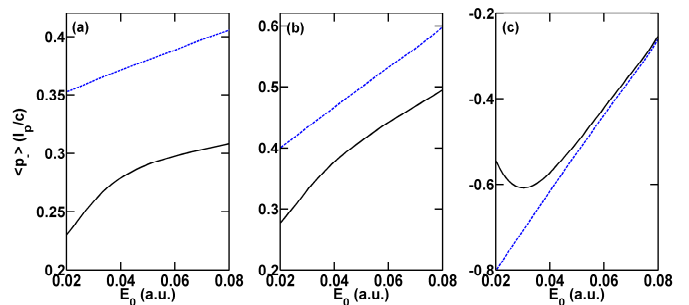


Figure 3. Asymptotic light-front momentum $\langle p_- \rangle$ vs E_0 . The initial states are (a) hydrogen atom with quantum numbers $(1, 0, 0)$, (b) argon with $(3, 1, 1)$, and (c) with $(3, 1, 0)$. The solid black lines include the continuum and the sub-barrier CC, while the dashed blue lines only the sub-barrier CC.

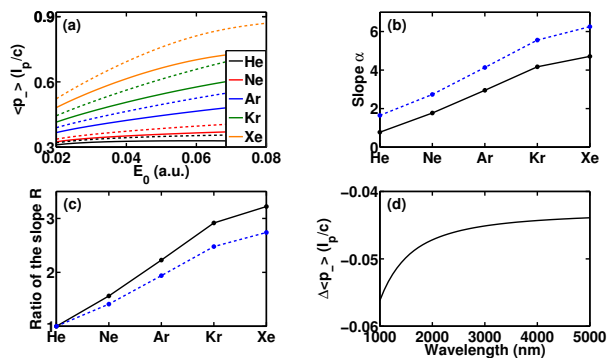


Figure 4. (a) Focal averaged $\langle p_- \rangle$ vs E_0 for different atomic species; (b) The slope α of the field dependence of $\langle p_- \rangle$; (c) The scaled ratio of the slope $R \equiv (\alpha + 1)/(\alpha_{\text{He}} + 1)$ with respect to the case of a helium atom (as an example); (d) The longitudinal momentum shift due to the continuum CC vs wavelength at a laser intensity of 10^{14} W/cm 2 . The solid lines include the full CC, while the dashed lines only the sub-barrier CC.

two peaks around $\pm\sqrt{E_0/\kappa}$ for $(3, 1, 0)$, which originate from the momentum distribution of the initial bound state, see Fig. 2(c,d). In the dipole theory, the two peaks are equally probable and $\langle p_- \rangle = 0$. The center of the window \mathcal{W} is at $v_{zs} = -2I_p/(3c)$ in the nondipole theory. The asymmetry of the window with respect to the origin results in suppression of the probability of the positive peak with respect to the negative one, yielding a negative longitudinal momentum $\langle p_- \rangle < 0$. After accounting for the atomic Coulomb field, the peaks of the wave function become closer, which results in an increase of the PMD peaks and in decreasing the asymmetry between them. The sub-barrier CC for the right peak is larger [Fig. 1(f)], which leads to a decrease of $\langle p_- \rangle$ by absolute value. Hence for the state $(3, 1, 0)$, the exponent of Eq. (4) prefers the peak $p_- \approx -\sqrt{E_0/\kappa}$ due to the nondipole momentum shift I_p/c , while the prefactor prefers the peak $p_- \approx \sqrt{E_0/\kappa}$ due to the sub-barrier Coulomb field effect.

Next let us discuss the role of the Coulomb field in the continuum, see Fig. 3. $P = (p_x, p_y, p_-)$ is no longer conserved and the momentum is reduced by absolute value as a result of the Coulomb momentum transfer mostly at the tunnel exit. For the states $(1, 0, 0)$ (hydrogen) and $(3, 1, \pm 1)$ (argon) the continuum CC decreases the momentum shift, however, approximately maintaining the slope of the field dependence [50]. For a smaller electric field strength, the tunneling exit is farther away from the atomic core, while the photoelectron can stay a longer time around the nuclei. As a consequence, $\langle p_- \rangle$ decreases more significantly in the absolute value, while the slope of the curve remains less affected. Thus, the sub-barrier Coulomb dynamics induces a quite strong field dependence in the nondipole longitudinal momentum shift (a large slope vs the laser field) distinguishable in

an experiment as discussed below.

As a distinctive feature of the sub-barrier CC, we suggest comparing the longitudinal momentum shifts as well as the slopes of the field dependence α for different atomic species, see Fig. 4(a). The qualitatively robust signature of the sub-barrier CC is the increase of $\langle p_- \rangle$ and its slope α with a higher principal quantum number of the active electron. We have $\langle p_- \rangle \sim \alpha \frac{E_0 I_p}{E_a c}$, and the qualitative behavior does not change when including the continuum CC, as one can see from Fig. 4 (a)-(b). Moreover, we can define the scaled ratio of the slope $R \equiv (\alpha + 1)/(\alpha_{\text{He}} + 1)$ with respect to the case of a helium atom (as an example), which shows less dependence on the continuum CC [Fig. 4(c)]. Thus, the comparison of the longitudinal momentum shift for different atoms can unambiguously confirm the signature of the sub-barrier CC in an experiment. The qualitative signature is also robust to the focal averaging. The longer laser wavelengths are more beneficial for the observation of the considered effects, as the masking effect of nonadiabaticity can be avoided at $\gamma < 1$, see Fig. 4(d), which shows an increase of the continuum CC due to nonadiabaticity at shorter wavelengths.

The discussed effect can be confirmed with currently available experimental conditions. For instance, the deviation of the momentum shift from $I_p/(3c)$ in the case of xenon atoms is $\delta \langle p_- \rangle \approx 0.3I_p/c \approx 10^{-3}$ a.u. at $E_0 = 0.06$ a.u., which is detectable with momentum resolution achieved in experiments of Refs. [14, 15]. In these experiments, an average momentum shift $\langle p_- \rangle \approx I_p/(3c) \sim 10^{-3}$ a.u. is distinguished in argon and xenon. Thus, we may conclude that the experimental capabilities similar to Refs. [14, 15] are sufficient to detect the discussed effect. However, one will need to collect more data with different atoms and with a large range of accessible laser intensities.

Concluding, after introducing the light-front non-dipole Coulomb-corrected theory, we reveal a counterintuitive role of the Coulomb field of the atomic core in nondipole sub-barrier dynamics, which increases the photoelectron nondipole momentum shift despite its attractive nature, with consequences for the momentum partition of the absorbed laser photons. We demonstrate, disentangling the sub-barrier and continuum effects, that the Coulomb sub-barrier signatures can be observed in the asymptotic momentum distribution with long-wavelength laser fields by measuring the characteristic slope of the field dependence of the average longitudinal momentum in different gas targets.

P.-L. H. acknowledges support via the prize of the Shanghai Jiao Tong University for outstanding graduate students.

* peilun@mpi-hd.mpg.de

[†] k.hatsagortsyan@mpi-hd.mpg.de

- [1] A. L'Huillier and P. Balcou, High-order harmonic generation in rare gases with a 1-ps 1053-nm laser, *Phys. Rev. Lett.* **70**, 774 (1993).
- [2] P. B. Corkum, Plasma perspective on strong field multiphoton ionization, *Phys. Rev. Lett.* **71**, 1994 (1993).
- [3] P. Agostini, F. Fabre, G. Mainfray, G. Petite, and N. K. Rahman, Free-free transitions following six-photon ionization of xenon atoms, *Phys. Rev. Lett.* **42**, 1127 (1979).
- [4] A. L'Huillier, L. A. Lompre, G. Mainfray, and C. Manus, Multiply charged ions induced by multiphoton absorption in rare gases at 0.53 μm , *Phys. Rev. A* **27**, 2503 (1983).
- [5] L. Marrucci, C. Manzo, and D. Paparo, Optical spin-to-orbital angular momentum conversion in inhomogeneous anisotropic media, *Phys. Rev. Lett.* **96**, 163905 (2006).
- [6] Y.-Y. Chen, J.-X. Li, K. Z. Hatsagortsyan, and C. H. Keitel, γ -ray beams with large orbital angular momentum via nonlinear Compton scattering with radiation reaction, *Phys. Rev. Lett.* **121**, 074801 (2018).
- [7] I. Barth and O. Smirnova, Nonadiabatic tunneling in circularly polarized laser fields: Physical picture and calculations, *Phys. Rev. A* **84**, 063415 (2011).
- [8] A. Hartung, F. Morales, M. Kunitski, K. Henrichs, A. Laucke, M. Richter, T. Jahnke, A. Kalinin, M. Schöffler, L. P. H. Schmidt, *et al.*, Electron spin polarization in strong-field ionization of xenon atoms, *Nat. Photon.* **10**, 526 (2016).
- [9] Y.-F. Li, Y.-Y. Chen, W.-M. Wang, and H.-S. Hu, Production of highly polarized positron beams via helicity transfer from polarized electrons in a strong laser field, *Phys. Rev. Lett.* **125**, 044802 (2020).
- [10] Z. Chen, P.-L. He, and F. He, Spiral nuclear momentum distribution for the dissociation of h_2^+ in a circularly polarized laser pulse, *Physical Review A* **101**, 033406 (2020).
- [11] C. T. L. Smeenk, L. Arissian, B. Zhou, A. Mysyrowicz, D. M. Villeneuve, A. Staudte, and P. B. Corkum, Partitioning of the linear photon momentum in multiphoton ionization, *Phys. Rev. Lett.* **106**, 193002 (2011).
- [12] A. Ludwig, J. Maurer, B. W. Mayer, C. R. Phillips, L. Gallmann, and U. Keller, Breakdown of the dipole approximation in strong-field ionization, *Phys. Rev. Lett.* **113**, 243001 (2014).
- [13] J. Maurer, B. Willenberg, J. Daněk, B. W. Mayer, C. R. Phillips, L. Gallmann, M. Klaiber, K. Z. Hatsagortsyan, C. H. Keitel, and U. Keller, Probing the ionization wave packet and recollision dynamics with an elliptically polarized strong laser field in the nondipole regime, *Phys. Rev. A* **97**, 013404 (2018).
- [14] A. Hartung, S. Eckart, S. Brennecke, J. Rist, D. Trabert, K. Fehre, M. Richter, H. Sann, S. Zeller, K. Henrichs, *et al.*, Magnetic fields alter strong-field ionization, *Nat. Phys.* **15**, 1222 (2019).
- [15] B. Willenberg, J. Maurer, B. W. Mayer, and U. Keller, Sub-cycle time resolution of multi-photon momentum transfer in strong-field ionization, *Nature communications* **10**, 1 (2019).
- [16] N. Haram, I. Ivanov, H. Xu, K. T. Kim, A. Atia-tul Noor, U. S. Sainadh, R. D. Glover, D. Chetty, I. V. Litvinyuk, and R. T. Sang, Relativistic nondipole effects in strong-field atomic ionization at moderate intensities, *Phys. Rev. Lett.* **123**, 093201 (2019).
- [17] S. Grundmann, D. Trabert, K. Fehre, N. Strenger, A. Pier, L. Kaiser, M. Kircher, M. Weller, S. Eckart, L. P. H. Schmidt, F. Trinter, T. Jahnke, M. S. Schöffler, and R. Dörner, Zeptosecond birth time delay in molecular photoionization, *Science* **370**, 339 (2020).
- [18] A. Hartung, S. Brennecke, K. Lin, D. Trabert, K. Fehre, J. Rist, M. S. Schöffler, T. Jahnke, L. P. H. Schmidt, M. Kunitski, M. Lein, R. Dörner, and S. Eckart, Electric nondipole effect in strong-field ionization, *Phys. Rev. Lett.* **126**, 053202 (2021).
- [19] S. Grundmann, I. Kircher, M. and Vela-Perez, G. Nalin, D. Trabert, N. Anders, N. Melzer, J. Rist, A. Pier, N. Strenger, *et al.*, Observation of photoion backward emission in photoionization of He and N_2 , *Phys. Rev. Lett.* **124**, 233201 (2020).
- [20] D. Cricchio, E. Fiordilino, and K. Z. Hatsagortsyan, Momentum partition between constituents of exotic atoms during laser-induced tunneling ionization, *Phys. Rev. A* **92**, 023408 (2015).
- [21] M. Klaiber, E. Yakaboylu, H. Bauke, K. Z. Hatsagortsyan, and C. H. Keitel, Under-the-barrier dynamics in laser-induced relativistic tunneling, *Phys. Rev. Lett.* **110**, 153004 (2013).
- [22] E. Yakaboylu, M. Klaiber, H. Bauke, K. Z. Hatsagortsyan, and C. H. Keitel, Relativistic features and time delay of laser-induced tunnel ionization, *Phys. Rev. A* **88**, 063421 (2013).
- [23] A. M. Perelomov, V. S. Popov, and M. V. Terent'ev, Ionization of atoms in an alternating electric field, *Sov. Phys. JETP* **23**, 924 (1966).
- [24] A. M. Perelomov and V. S. Popov, Ionization of atoms in an alternating electric field. III, *Sov. Phys. JETP* **25**, 336 (1967).
- [25] M. V. Ammosov, N. B. Delone, and V. P. Krainov, Tunnel ionization of complex atoms and of atomic ions in an alternating electromagnetic field, *Zh. Eksp. Teor. Fiz.* **91**, 2008 (1986).
- [26] C. I. Blaga, F. Catoire, P. Colosimo, G. G. Paulus, H. G. Muller, P. Agostini, and L. F. DiMauro, Strong-field photoionization revisited, *Nat. Phys.* **5**, 335 (2009).
- [27] W. Quan, Z. Lin, M. Wu, H. Kang, H. Liu, X. Liu, J. Chen, J. Liu, X. T. He, S. G. Chen, *et al.*, Classical aspects in above-threshold ionization with a midinfrared strong laser field, *Phys. Rev. Lett.* **103**, 093001 (2009).
- [28] H. Liu, Y. Liu, L. Fu, G. Xin, D. Ye, J. Liu, X. T. He, Y. Yang, X. Liu, Y. Deng, C. Wu, and Q. Gong, Low yield of near-zero-momentum electrons and partial atomic stabilization in strong-field tunneling ionization., *Phys. Rev. Lett.* **109**, 093001 (2012).
- [29] B. Wolter, M. G. Pullen, M. Baudisch, M. Sclafani, M. Hemmer, A. Senftleben, C. D. Schröter, J. Ullrich, R. Moshhammer, and J. Biegert, Strong-field physics with mid-ir fields, *Phys. Rev. X* **5**, 021034 (2015).
- [30] C. Liu and K. Z. Hatsagortsyan, Origin of unexpected low energy structure in photoelectron spectra induced by midinfrared strong laser fields, *Phys. Rev. Lett.* **105**, 113003 (2010).
- [31] T.-M. Yan, S. V. Popruzhenko, M. J. J. Vrakking, and D. Bauer, Low-energy structures in strong field ionization revealed by quantum orbits, *Phys. Rev. Lett.* **105**, 253002 (2010).
- [32] A. Kästner, U. Saalman, and J. M. Rost, Electron-energy bunching in laser-driven soft recollisions, *Phys. Rev. Lett.* **108**, 033201 (2012).
- [33] T. Keil, S. V. Popruzhenko, and D. Bauer, Laser-driven recollisions under the Coulomb barrier, *Phys. Rev. Lett.*

- 117**, 243003 (2016).
- [34] P.-L. He, M. Klaiber, K. Z. Hatsagortsyan, and C. H. Keitel, High-energy direct photoelectron spectroscopy in strong-field ionization, *Phys. Rev. A* **98**, 053428 (2018).
- [35] M. Førre, J. P. Hansen, L. Kocbach, S. Selstø, and L. B. Madsen, Nondipole ionization dynamics of atoms in superintense high-frequency attosecond pulses, *Phys. Rev. Lett.* **97**, 043601 (2006).
- [36] J. Daněk, M. Klaiber, K. Z. Hatsagortsyan, C. H. Keitel, B. Willenberg, J. Maurer, B. W. Mayer, C. R. Phillips, L. Gallmann, and U. Keller, Interplay between coulomb-focusing and non-dipole effects in strong-field ionization with elliptical polarization, *J. Phys. B* **51**, 114001 (2018).
- [37] J. Daněk, K. Z. Hatsagortsyan, and C. H. Keitel, Analytical approach to coulomb focusing in strong-field ionization. i. nondipole effects, *Physical Review A* **97**, 063409 (2018).
- [38] B. Willenberg, J. Maurer, U. Keller, J. Daněk, M. Klaiber, N. Teeny, K. Z. Hatsagortsyan, and C. H. Keitel, Holographic interferences in strong-field ionization beyond the dipole approximation: The influence of the peak and focal-volume-averaged laser intensities, *Phys. Rev. A* **100**, 033417 (2019).
- [39] T.-M. Yan and D. Bauer, Sub-barrier coulomb effects on the interference pattern in tunneling-ionization photoelectron spectra, *Phys. Rev. A* **86**, 053403 (2012).
- [40] M. Klaiber, K. Z. Hatsagortsyan, and C. H. Keitel, Under-the-tunneling-barrier recollisions in strong-field ionization, *Phys. Rev. Lett.* **120**, 013201 (2018).
- [41] S. Chelkowski, A. D. Bandrauk, and P. B. Corkum, Photon momentum sharing between an electron and an ion in photoionization: from one-photon (photoelectric effect) to multiphoton absorption, *Phys. Rev. Lett.* **113**, 263005 (2014).
- [42] S. Chelkowski, A. D. Bandrauk, and P. B. Corkum, Photon-momentum transfer in multiphoton ionization and in time-resolved holography with photoelectrons, *Phys. Rev. A* **92**, 051401 (2015).
- [43] S. Chelkowski, A. D. Bandrauk, and P. B. Corkum, Photon-momentum transfer in photoionization: From few photons to many, *Phys. Rev. A* **95**, 053402 (2017).
- [44] P. A. M. Dirac, Forms of relativistic dynamics, *Rev. Mod. Phys.* **21**, 392 (1949).
- [45] H. Reiss, Theoretical methods in quantum optics: S-matrix and Keldysh techniques for strong-field processes, *Prog. Quant. El.* **16**, 1 (1992).
- [46] V. S. Popov, V. D. Mur, and B. M. Karnakov, The imaginary-time method for relativistic problems, *Sov. Phys. JETP Lett.* **66**, 229 (1997).
- [47] V. D. Mur, B. M. Karnakov, and V. S. Popov, Relativistic version of the imaginary-time formalism, *Sov. Phys. JETP Lett.* **87**, 433 (1998).
- [48] N. Milosevic, V. P. Krainov, and T. Brabec, Semiclassical dirac theory of tunnel ionization, *Phys. Rev. Lett.* **89**, 193001 (2002).
- [49] M. Klaiber, E. Yakaboylu, and K. Z. Hatsagortsyan, Above-threshold ionization with highly charged ions in superstrong laser fields. ii. relativistic coulomb-corrected strong-field approximation, *Phys. Rev. A* **87**, 023418 (2013).
- [50] See the Supplemental Materials for the details.
- [51] P.-L. He, D. Lao, and F. He, Strong field theories beyond dipole approximations in nonrelativistic regimes, *Phys. Rev. Lett.* **118**, 163203 (2017).
- [52] H. Ni, S. Brennecke, X. Gao, P.-L. He, S. Donsa, I. Brezinová, F. He, J. Wu, M. Lein, X.-M. Tong, and J. Burgdörfer, Theory of Subcycle Linear Momentum Transfer in Strong-Field Tunneling Ionization, *Phys. Rev. Lett.* **125**, 073202 (2020).
- [53] M. Klaiber, J. Daněk, E. Yakaboylu, K. Z. Hatsagortsyan, and C. H. Keitel, Strong-field ionization via a high-order coulomb-corrected strong-field approximation, *Physical Review A* **95**, 023403 (2017).
- [54] However, the CC in x -direction increases the nondipole momentum shift (this corrects the simple estimate in [22]), but the sub-barrier z -dynamics compensates that.